Available online at www.sciencedirect.com

ScienceDirect

Procedia Engineering 141 (2016) 32 – 37

Procedia Engineering

www.elsevier.com/locate/procedia

MRS Singapore – ICMAT Symposia Proceedings

8th International Conference on Materials for Advanced Technologies

Synthesis of iron sulfide and iron oxide nanocrystal thin films for green energy applications

Hongfei Liu*, Dongzhi Chi

*Institute of Materials Research and Engineering (IMRE), A*STAR (Agency for Science, Technology and Research), 3 Research Link, Singapore 117602, Singapore*

Abstract

Solar radiation and hydrogen generation via splitting water molecules have been recognized as sustainable and clean energy sources having great industrial potentials. In this regard, thin film materials for photovoltaic and photoanodes applications have been widely developed in the last decade. For thin film photovoltaic applications, taking material availability, extraction/processing cost, energy conversion efficiency, and eco-friendliness into account, FeS_2 (pyrite) has been predicted to hold the leading position among the most plausible candidates such as Cu_2S, Cu_2O, CuO, etc. On the other hand, feasible water splitting on nanostructured surface and/or hybrid nanostructures has been observed in the last few years. In terms of processing cost, feasibility in scale-up for mass production, material engineering for efficiency, etc., physical vapor depositions (PVDs), e.g., magnetron-sputtering deposition, have great advantages. Here, we present our recent studies on synthesis of iron sulfide and oxide layered and nanostructured films by combining PVD and thermal vapor sulfurization/oxidation techniques.

Selection and/or peer-review under responsibility of the scientific committee of Symposium 2015 ICMAT

Keywords: Thermal vapor sulfurization; thin film deposition; photovoltaic; water-splitting

1. Introduction

Iron-VI compounds, such as iron sulfide and iron oxide, are important functional materials and have attracted considerable experimental and theoretical interests in the past decades. The unique physical properties of the

* Corresponding author. Tel.: +65-68748047; fax: +65-68747744.
E-mail address: liuhf@imre.a-star.edu.sg

Selection and/or peer-review under responsibility of the scientific committee of Symposium 2015 ICMAT
doi:10.1016/j.proeng.2015.08.1104

nonmagnetic semiconductor FeS_2 (pyrite) have made it a potential photovoltaic (PV) absorber with high-efficiency and low-cost [1]. The magnetic half-metal Fe_3S_4 (greigite) and Fe_3O_4 (magnetite) have the equivalent formula and the inverse cubic spinel structure, and their nanostructures have proved extremely important in ultrahigh-density magnetic storages [2], spintronic devices [3], and catalysts for protometabolism [4]. Feasible water splitting on the surface of composite catalyst/α-Fe_2O_3 photoanodes and crystalline Fe_3O_4 surface to generate hydrogen, which has been recognized as another potential clean energy source beside solar radiation, have also been observed in the last few years. In PV applications, the FeS_2 thin films are generally synthesized either by crystal growth, e.g., molecular beam epitaxy (MBE), metal-organic chemical vapor deposition (MOCVD), magnetron-sputtering, etc., or by sulfurizing Fe and/or Fe-content compound thin films. In contrast, the synthesis of Fe_3O_4 and Fe_3S_4 for water splitting or other electrochemical applications is dominant by chemical bath depositions (CBDs). In the case of sulfurizing, Fe_3S_4 is a natural intermediate on the polysulfide pathway to FeS_2. Fe_3S_4 is also feasibly converted into Fe_3O_4 due to their equivalent formula and the inverse cubic spinel structure. In this paper we report on the conversion of Fe_3S_4 to both FeS_2 and Fe_3O_4 by using a horizontal tube-furnace thermal treatment system. For these studies, we have employed x-ray diffraction (XRD), back-scattering Raman spectroscopy, and scanning-electron microscopy (SEM).

2. Experiments

2.1. Magnetron sputtering deposition of Fe_3S_4 thin films

The nanocrystal Fe_3S_4 thin films with various thicknesses were deposited on Si and glass substrates at room temperature using a dc-magnetron sputtering technology. During the sputtering deposition, pure argon (> 99.999%) was used as the working gas; the gas flow rate and the work pressure were set at 10 SCCM and 4×10^{-3} Torr, respectively. Before sputtering, the chamber was pumped down to ~2×10^{-6} Torr with the help of a liquid-nitrogen cooling system to minimize the undesired contaminations. A commercial (Super Conductor Materials, Inc.) 3-inch conductive $Fe_{0.95}S_{1.05}$ (99.99%) target was used as the source material. The dc-power applied on the target was ~ 100 W, which led to a growth rate of about 0.2-nm/s under certain sputtering conditions. Before loading into the sputtering deposition chamber, the Si substrates were etched in a buffered hydrofluoride solution followed by cleaning in deionized water to remove the native oxide skin layer. The glass substrates were cleaned by sinking in a mixture of H_2O_2 and H_2SO_4 (1:3) heated at 120 °C for 20 minutes.

2.2. Sulfurizing and oxidation of Fe_3S_4 thin films

Post-growth thermal treatment (i.e., sulfurizing and oxidation) of the Fe_3S_4 thin films were carried out in a tube-furnace system, which is schematically shown in Fig. 1. The detailed experiment procedures can be found in our earlier publications [5, 6]. It should be noted here that there was no oxygen source intentionally supplied during the oxidation process [see Fig. 1(b)]. The phenomenon of thermal oxidation without supplying intentional oxygen has also been observed in our recent experiments for rapid thermal annealing of InN [7]. The sulfurization process was carried out at 400 °C for 2 hours while the oxidation was carried out at 350~550 °C for 2 hours.

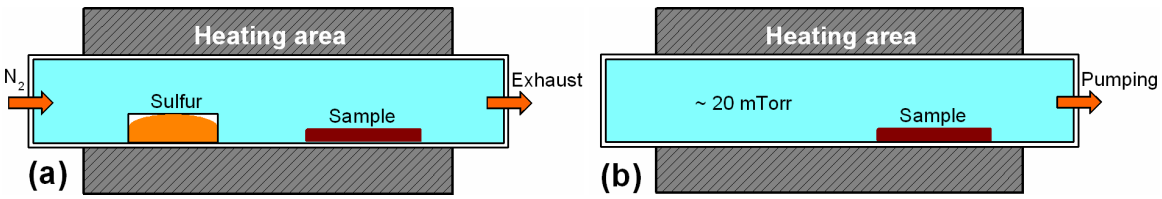

Fig. 1. Schematic diagrams of the tube-furnace system used for the sulfurizing (a) and oxidation (b) of Fe_3S_4 to generate FeS_2 and Fe_3O_4, respectively.

Before and after the sulfurization/oxidation, the thin film samples were characterized by employing a general-area-detector XRD system (GADDS, Bruker-D8), which has the great advantage of being highly sensitive to crystal phase structures. Raman scattering was carried out at room temperature using a 488-nm laser as the excitation source in a backscattering configuration. The surface morphology evolutions were recorded by using a field-emission SEM (JEOL JSM-6700).

3. Results and discussion

3.1. Deposition of Fe_3S_4 thin films

Figure 2(a) shows the XRD curves measured from the sputter-target and a 1.3-μm thin film deposited on Si using the target. The patterns, shown together with the XRD curves in Fig. 2(a), are the best matched ones that were automatically searched out from the JCPDS database. The XRD curves and their matched patterns reveal that the target material is basically $Fe_{0.95}S_{1.05}$ while the film deposited from the target atop the substrate under the chosen sputtering deposition conditions is Fe_3S_4. It has to be noted that the XRD curves collected from the films with thicknesses smaller than 100 nm do not exhibit any diffraction features most likely due to the undeveloped crystallizations at room temperature [8]. The increased S-to-Fe ratio in the film (1.33) as compared to that in the target material (1.11) implies that the sputter yield of S is larger than that of Fe, most likely due to the light atom of S and the magnetic property of Fe. An increase of sulfur incorporation in the target material led to target powdering during the magnetron-sputtering manifested itself by sparking and flashing of the arcing. It is also found that an increase in the film thickness will give rise to film cracking. In this regard, the films used in the post-growth thermal annealing/processing are generally thinner than 1.3 μm. Figure 2(b) shows the top-viewed SEM image recorded from the 1.3-μm thick Fe_3S_4 film. It is clearly seen that rice-shape-like clusters, consisting of nanoscale crystals, were formed in the film.

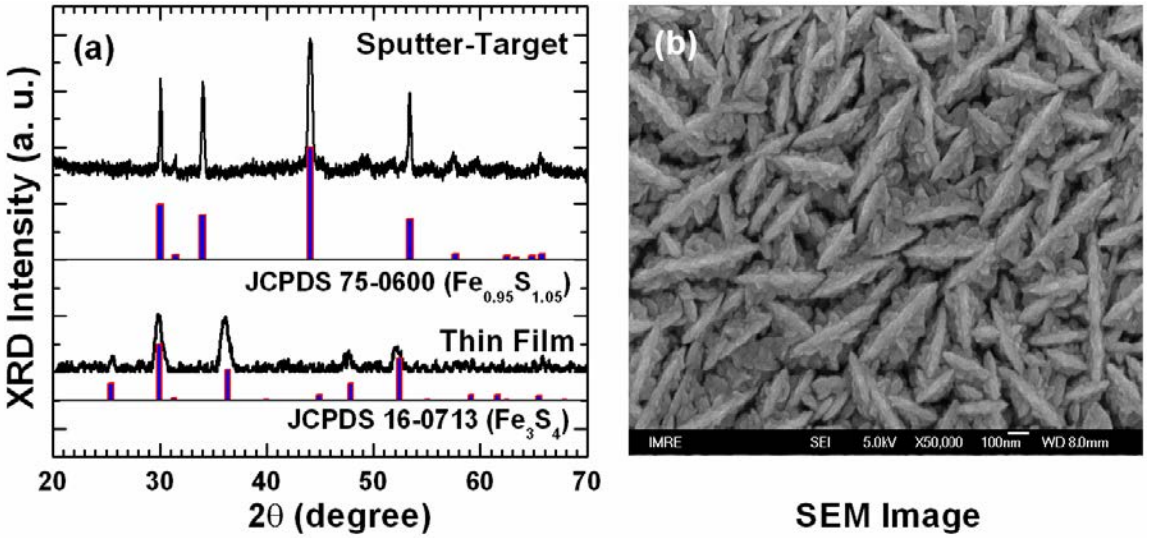

Fig. 2. (a) XRD curves collected from the sputter-target and the thin film deposited from the target onto a silicon substrate using the chosen sputtering deposition parameters, the patterns are the best matches found out from the JCPDF database; (b) top-viewed SEM image recorded from the as-deposited Fe_3S_4 film with the nominal thickness of 1.3 μm, showing the rice-shape-like clusters consisted of nanoscale crystals.

3.2. Sulfurization of Fe_3S_4 thin films

Figures 3(a) and 3(b) present the XRD curves collected from the 100-nm and 500-nm thick Fe_3S_4 thin films, respectively, after their sulfurization. Likewise, the patterns shown together with the XRD curves are the best marches from the JCPDS database. It is clearly seen that both the *thin* and the *thick* films are completely converted into pyrite FeS_2 in a pure crystal-phase structure. Figures 3(c) and 3(d), which were recorded from the 500-nm thick film before and after sulfurization, show that the rice-shape-like structures have developed into a layered film with smooth surface and an increased packing density. We have mentioned above that the XRD curve of the as-deposited 100-nm thick Fe_3S_4 film does not exhibit any diffraction features. In comparison, the sharp and strength diffraction peaks in Fig. 3(a) reveal that the crystal quality of the thin film was greatly improved during the post-growth thermal sulfurization via rearrangement of atoms (i.e., recrystallization) at elevated temperatures [9]. As a consequence, the surface of thin film is smoothened and the packing density is enhanced as compared to the as-deposited Fe_3S_4 sample.

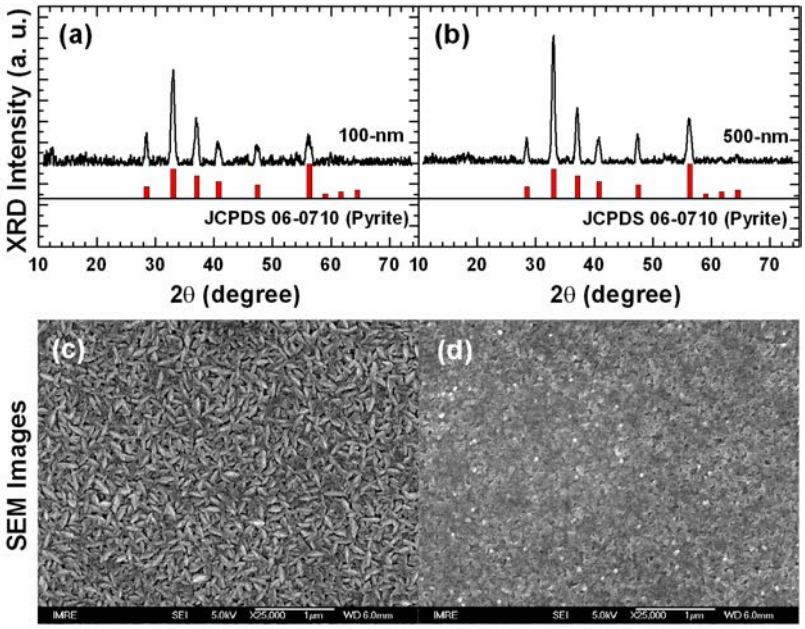

Fig. 3. XRD spectra collected from sulfurized Fe_3S_4 films with the thicknesses of (a) 100-nm and (b) 500-nm, the patterns are the best matches found out from the JCPDF data base; (c) and (d) are the SEM images recorded from the 500-nm sample before and after sulfurizing.

3.3. Oxidation of Fe_3S_4 thin films

Oxidation was carried out for a 1.3 μm thick Fe_3S_4 film at 350, 450, and 550 °C. Figures 4(a) and 4(b) show the XRD and Raman scattering spectral evolutions as a function of oxidation temperatures. The features indicated by asterisks are from Fe_3S_4. For the XRD curves, based on the best pattern matching using the JCPDS database, we found that the Fe_3S_4 nanocrystal film completely converted into Fe_3O_4 through Fe_7S_8. The evolution in diffraction peak intensities of both Fe_7S_8 and Fe_3O_4, when the oxidation temperature is increased, reveals that the reaction of Fe_3S_4 with oxygen at elevated temperatures to generate Fe_7S_8 and Fe_3O_4 occurred simultaneously, especially at lower oxidation temperature. When the oxidation temperature is further increased, the reaction of Fe_7S_8 with oxygen generates Fe_3O_4. No intermediate crystal-phase structure other than Fe_7S_8 was observed on the pathway from Fe_3S_4 to Fe_3O_4. The increase in the diffraction peak intensities of Fe_3O_4 also indicates the improvement in crystal quality at

higher oxidation temperatures. This result is also consistent with the Raman scattering spectral evolutions in Fig. 4(b), where the Raman features, typically T_{2g} (2), T_{2g} (3), and A_{1g} of Fe_3O_4 [10], monotonically increase in intensities with the increase in oxidation temperatures.

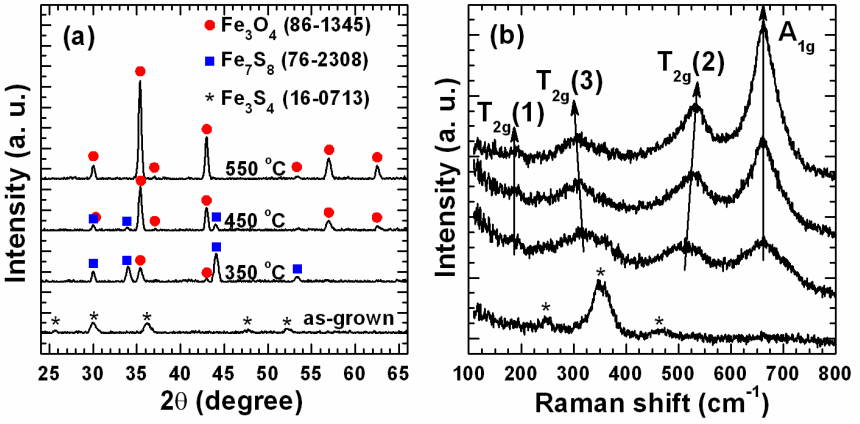

Fig. 4. XRD (a) and Raman scattering (b) spectral evolutions of Fe_3S_4 thin film (1.3-μm in thickness) upon post-growth thermal oxidation at 350, 450, and 550 °C. The Raman spectra were collected at room temperature using a 488-nm laser as the excitation source.

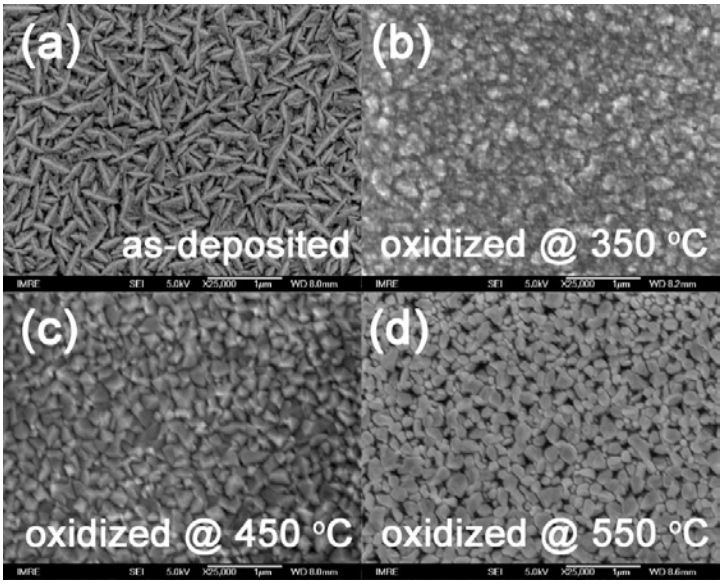

Fig. 5. SEM images recorded from a1.3-um thick nanocrystal Fe_3S_4 film (a) as-deposited, (b) oxidized at 350 °C, (c) oxidized at 450 °C, and (d) oxidized at 550 °C.

Presented in Fig. 5 are the morphology changes of the Fe_3S_4 thin film as a function of thermal oxidation temperatures increasing from 350, to 450 and 550 °C. It is seen that the thermal oxidation at lower temperature, i.e., 350 °C [Fig. 5(b)], somehow dissociated and totally modified the rice-shape-like clusters. The structural

morphologies of the low-temperature oxidized sample seem more like crystal grains of ~ 100 nm and fine particles of ~10-30 nm in diameters. When the oxidation temperature is increased to 450 °C, the crystal grains are much clearer and the grain sizes are increased [Fig. 5(c)]. Crystal facets can now be clearly observed. These facets correspond to adjacent {111} atomic planes of a cubic crystal [11]. The fine particles, as those observed in Fig. 5(a) and 5(b), have disappeared from Fig. 5(c). However, one can see in Fig. 5(c) that the grain sizes are not uniform and some small grains are distributed in between bigger ones. An additional increase in the oxidation temperature to 550 °C further increased the grain sizes [see Fig. 5(d)]. Meanwhile, those small grains that distributed in between bigger ones are now replaced by nanoscale pores. In terms of the XRD and Raman scattering results shown above in Fig. 4, the morphologies observed in Figs. 5(b), 5(c), and 5(d) are mainly from Fe_3O_4 grains. Based on the SEM observations, we may draw a conclusion that grains movement and coalescence of Fe_3O_4 occurred during the thermal oxidation, which led to the improvement in crystal quality, supporting the XRD and Raman scattering results.

4. Conclusion

In conclusion, Fe_3S_4 nanocrystal thin films have been deposited on Si and glass substrates by magnetron-sputtering at room temperature from a $Fe_{0.95}S_{1.05}$ target material. In a tube-furnace system with sulfur supplied in a crucible placed in the up-stream of the nitrogen carrier gas, the Fe_3S_4 thin film can be converted into pure FeS_2 without any other crystal-phase incorporation. In the same post-growth heat treatment system, without intentionally supplying any other source, the Fe_3S_4 thin film can be oxidized into Fe_3O_4. Fe_7S_8 is the dominant mediate crystal-phase on the pathway from Fe_3S_4 to Fe_3O_4 at relatively lower oxidation temperatures. At higher temperatures, Fe_3S_4 can be directly converted into Fe_3O_4. The obtained single phase nanocrystal FeS_2 thin film has great potential in photovoltaic application while both the Fe_3S_4 and Fe_3O_4 nanocrystal thin films might have important consequence in water-splitting for hydrogen generations.

References

[1] Wadia, C., Alivisatos, A. P., Kammen, D. M., 2009. Materials availability expands the opportunity for large-scale photovoltaics deployment, Environmental Science & Technology 43, p. 2072.
[2] Zeng, H., Li, J., Liu, J. P., Wang, Z. L., Sun, S., 2002. Exchange-coupled nanocomposite magnets by nanoparticle self-assembly, Nature 420, p. 395.
[3] Wolf, S. A., Awschalom, D. D., Buhrman, R. A., Daughton, J. M., von Molnár, S., Roukes, M. L., Chtchelkanova, A. Y., Treger, D. M., 2001. Spintronics: a spin-based electronics vision for the future, Science 294, p. 1488.
[4] Duderstadt, R. E., Brereton, P. S., Adams, M. W. W., Johnson, M. K., 1998. Spectroscopic evidence for a new type of [Fe_3S_4] cluster in a mutant form of Pyrococcus furiosus ferredoxin, Journal of American Chemistry Society 120, p. 8525.
[5] Liu, H., Chi, D., 2012. Magnetron-sputter deposition of Fe_3S_4 thin films and their conversion into pyrite (FeS_2) by thermal sulfurization for photovoltaic applications, Journal of Vacuum Science & Technology A 30, p. 04D102.
[6] Liu, H. F., Huang, A., Chi, D. Z., 2010. Thermal annealing of nanocrystalline Fe_3S_4 films deposited on Si substrates by dc-magnetron sputtering at room temperature, Journal of Physics D: Applied Physics 43, p. 455405.
[7] Liu, H. F., Chi, D. Z., Liu, W., 2012. Layer-by-layer oxidation of InN(0001) thin films into body-center cubic In_2O_3(111) by cycle rapid thermal annealing, CrystEngComm 14, p. 7140.
[8] E. Alfonso, J. Olaya, and G. Cubillos, Thin film growth through sputtering technique and its applications (Crystallization-Science and Technology, Ed. M. R. B. Andreeta, Intech.), Chapter 15.
[9] H. Fukuda, Rapid thermal processing for future semiconductor devices (Elsevier B.V. ©2013).
[10] Bersani, D., Lottici, P. P., Montenero, A., 1999. Micro-Raman investigation of iron oxide films and powders produced by sol-gel syntheses, Journal of Raman Spectroscopy 30, p. 355.
[11] L-r Meng, Weimeng Chen, Yiwei Tan, Lin Zou, Chinping Chen, Heping Zhou, Qing Peng, Yadong Li, Fe_3O_4 octahedral colloidal crystals, 2011. Nano Res. 4, p. 370.